Accepted Manuscript

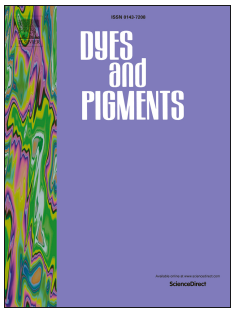

A julolidine-fused coumarin-NBD dyad for highly selective and sensitive detection of H_2S in biological samples

Ismail Ismail, Dawei Wang, Zhenghua Wang, Dan Wang, Changyu Zhang, Long Yi, Zhen Xi

PII: S0143-7208(18)32384-2

DOI: https://doi.org/10.1016/j.dyepig.2018.12.064

Reference: DYPI 7269

To appear in: *Dyes and Pigments*

Received Date: 28 October 2018

Revised Date: 19 December 2018

Accepted Date: 28 December 2018

Please cite this article as: Ismail I, Wang D, Wang Z, Wang D, Zhang C, Yi L, Xi Z, A julolidine-fused coumarin-NBD dyad for highly selective and sensitive detection of H_2S in biological samples, *Dyes and Pigments* (2019), doi: https://doi.org/10.1016/j.dyepig.2018.12.064.

A julolidine-fused coumarin-NBD dyad for highly selective and sensitive detection of H_2S in biological samples

Ismail Ismail,[a] Dawei Wang,[a] Zhenghua Wang,[a] Dan Wang,[a] Changyu Zhang,[b] Long Yi,[b,c*] and ZhenXi[a,c]*

[a]*State Key Laboratory of Elemento-Organic Chemistry, and Department of Chemical Biology, National Pesticide Engineering Research Center, College of Chemistry, Nankai University, Tianjin 300071, China. Fax: +86 022-23500952; Tel: +86 022-23504782. E-mail: zhenxi@nankai.edu.cn*

[b]*Beijing Key Laboratory of Bioprocess, Beijing University of Chemical Technology, 15 Beisanhuan East Road, Chaoyang District, Beijing 100029, China. E-mail: yilong@mail.buct.edu.cn*

[c]*Collaborative Innovation Center of Chemical Science and Engineering, Nankai University, Tianjin, China.*

A B S T R A C T

A new julolidine-fused coumarin-NBD probe **2** for H_2S detection is rationally designed based on the DFT caculations. This improved probe exhibits faster and larger *off-on* response as well as higher sensitivity compared with the previous coumarin-NBD probe **1**. Moreover, **2** possesses excellent selectivity and good biocompatibility, which can be employed to image H_2S in living cells and in zebrafish.

Keywords: Julolidine-fused coumarin-NBD probe, H_2S detection, Cell imaging, Zebrafish imaging

1. Introduction

H_2S has long been known as a toxic gas, but recent studies indicate that endogenously produced H_2S has important physiological functions, which is named as the third gasotransmitter after nitric oxide and carbon monoxide [1]. In mammals, endogenous H_2S could be enzymatically produced by three distinctive pathways, including cystathionine *β*-synthase (CBS), cystathionine *γ*-lyase (CSE), and 3-mercaptopyruvate sulfur-transferase (3-MST) along with cysteine aminotransferase (CAT) [2]. Accumulative evidence suggests that H_2S influences a wide range of physiological and pathological processes, including modulation of blood vessel tone and cardioprotection [3], endogenous stimulator of angiogenesis [4], and mitochondrial bioenergetics [5]. H_2S inhibits nuclear factor-*kB* activation in oxidized low-density lipoprotein-stimulated macrophage [6]. H_2S also plays an important role in tumor biology, and it is suggested that both inhibition of H_2S biosynthesis and elevation of H_2S concentration beyond a certain threshold could exert anticancer effects [4b,7]. In plants, H_2S participates in different processes including seed germination, plant growth, development and acquisition of stress tolerance [8-10]. Nevertheless, the pharmacological characters of H_2S and the precise mechanisms by which H_2S may be involved *in vivo* still remain largely unclear. Therefore, efficient tools for visualization of biological H_2S should be useful in further exploring H_2S biology and even for diagnosis of H_2S-related diseases.

Fluorescence-based method has recently emerged as an efficient approach for *in-situ* and real-time detection of H_2S in living biological systems [11-19]. One major challenge in the development of H_2S probes is the discovery of a chemical reaction to effectively separate the reactivity of biothiols and H_2S in auqeous buffer. To address this challenge, chemical reactions including nucleophilic addition [12], H_2S-triggered reduction [13], copper precipitation [14], thiolysis of dinitrophenyl ether [15], cleavage of C-N bonds (NBD amines) [16], thiolysis of NBD ethers/thioethers [17] and cleavage of C=C bonds [18] have been successfully employed to develop these molecular probes. For example, we reported the first H_2S-specific fluorescence probe

1 based on cleavage of C-N bonds [16a]. Stoke shift, limit of detection (LOD) and turn-on fluorescence fold (FI) of the probe **1** were 75 nm, 9 μM, and 45-fold, respectively, which are potentially disadvantage for sensing the biological H_2S that normally exists in the submicromolar level range.

Recently, Grimm et al. showed that replacing the N,N-dialkyl group with azetidine group can greatly improve the brightness and quantum yield of the fluorophores [22]. Yang et al. reported that blocking the twisting N,N-diethylamino group of coumarin can improve the fluorescence properties of the fluorophore, and in turn, enhance sensing performances [23]. We envision that such twisting N,N-diethylamino group of coumarin could also be employed for the development of improved NBD-based probe. Herein, we rationally design a new julolidine-fused coumarin-NBD probe **2** for H_2S detection (Scheme. 1). To our delight, the probe **2** showed excellent sensing performances with green-light emitting and was successfully used for bioimaging in living cells and in zebrafish.

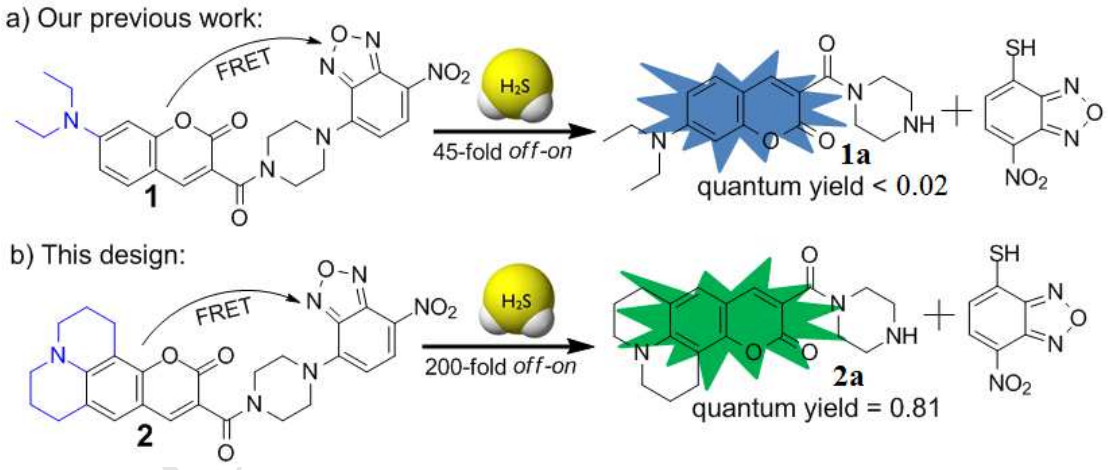

Scheme. 1 Rational design of an improved fluorescence probe for H_2S detection based on the thiolysis of NBD amine. a) The probe **1** was used for H_2S-specific detection with production of blue-emitting **1a** [16a]. b) The julolidine-fused coumarin-NBD dyad **2** was used for H_2S-specific detection with production of green-emitting **2a** and more than 200-fold *off-on* response during H_2S activation.

2. Experimental section

2.1. Reagents and apparatus

All chemicals and solvents used for synthesis were purchased from commercial suppliers and used directly in the experiment without further purification (J&K Scientific Ltd., Beijing, China). ^{1}H NMR and ^{13}C NMR spectra were recorded on a Bruker 400 spectrometer with $CDCl_3$, CD_2Cl_2 or DMSO-d_6 as solvent. Chemical shifts are reported in parts per million, relative to internal standard tetramethylsilane (δ = 0.00 ppm). High-resolution mass spectra (HRMS) were obtained on a 6520 Q-TOF LC/MS (Agilent, Santa Clara, CA). The UV-visible spectra were recorded on a CARY 100 Bio (Varian, USA). Fluorescence study was carried out using Varian Cary Eclipse spectrophotometer at 25 °C. The cells/zebrafish bioimaging were performed on a confocal microscope (Olympus FV1000 UPLSAPO40X).

*2.2. Synthesis of probe**2***

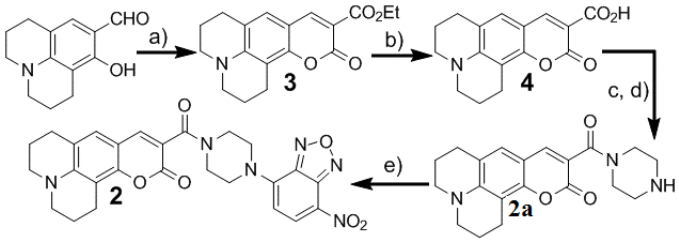

Scheme 2. Synthesis route for probe **2**. Reagents and conditions: a) diethyl malonate, piperidine, CH_3CN, reflux; b) Conc. HCl; c) 1-boc-piperazine, DCC, DMAP, CH_2Cl_2; d) trifluoroacetic acid, CH_2Cl_2; e) 4-chloro-7-nitro-1,2,3-benzoxadiazole, Et_3N, CH_2Cl_2.

A solution of 8-hydroxyjulolidine-9-carboxaldehyde (4.36 g, 20 mmol), diethyl malonate (6.41 g, 40 mmol) and piperidine (2 mL) in ethanol (60 mL) was refluxed for 24 h. After cooled to room temperature, the solvent was evaporated under vacuum and the resulting residue was purified by column chromatography (petroleum ether: ethyl acetate = 4: 1, v/v), yielding an orange solid **3** (4.95 g, 79%); mp 139-141 ºC;^{1}H NMR (400 MHz, DMSO-d_6) δ 8.38 (s, 1H), 7.17 (s, 1H), 4.21 (q, J = 7.2 Hz, 2H), 3.34-3.28 (m, 4H), 2.75-2.64 (m, 4H), 1.93-1.80 (m, 4H), 1.27 (t, J = 7.2 Hz, 3H).

A solution of **3** (2.0 g, 6.38 mmol) in concentrated HCl solution (20 mL) was stirred at 25 ºC for 24 h. After the reaction was completed, water (100 mL) was added to the solution. The mixture was extracted by ethyl acetate (50 mL) for three times, the combined organic layer was washed by H_2O (50 mL) and brine, dried over

anhydrous Na_2SO_4 and concentered under reduced pressure to afford compound **4** as orange solid (1.55 g, 85%), mp 223-225 ºC, ^{1}H NMR (400 MHz, DMSO-d_6) δ 12.20 (bs, 1H), 8.46 (s, 1H), 7.24 (s, 1H), 2.72 (dd, J = 13.2, 6.8 Hz, 4H), 2.51-2.50 (m, 4H), 1.95-1.81 (m, 4H).

A solution of **4** (1.0 g, 3.5 mmol), 1-boc-piperazine (0.65 g, 3.5 mmol), DCC (1.1 g, 5.26 mmol) and DMAP (4.9 mg, 0.04 mmol) in CH_2Cl_2 (20 mL) was stirred at room temperature for 12 h. After the reaction was completed, the precipitation was filtrated, and the solvent was removed under reduced pressure. The resulting residue was subjected to column chromatography on silica, yielding a yellow solid powder (1.46 g, 92%), which was further treated with 40 mL TFA/CH_2Cl_2 (v/v= 1/1). After stirred at room temperature for 3 h, the solvent was removed under the reduced pressure and the residue was purified by the column to afford intermediate **2a** (0.65 g, yield 83%), mp 185-187 ºC, ^{1}H NMR (400 MHz, $CDCl_3$) δ 7.81 (s, 1H), 6.90 (s, 1H), 3.86 (bs, 2H), 3.50 (bs, 2H), 3.31 (dd, J = 10.8, 5.2 Hz, 4H), 3.09 (bs, 4H), 2.87 (t, J = 6.4 Hz, 2H), 2.76 (t, J = 6.4 Hz, 2H), 2.02-1.92 (m, 4H). HRMS (ESI): m/z 354.1815 $[M+H]^+$ (calcd for $C_{20}H_{24}N_3O_3^+$, 354.1812).

A mixture of intermediate **2a** (130 mg, 0.37 mmol), NBD-Cl (73.4 mg, 0.37 mmol) and Et_3N (100 μL) in CH_2Cl_2 (20 mL) was stirred at room temperature overnight. After removed the solvent under reduced pressure, the resulting residue was subjected to column chromatography on silica (1% MeOH in CH_2Cl_2), yielding a red solid **2** (173 mg, 91%), mp 249-251 ºC, ^{1}H NMR (400 MHz, CD_2Cl_2) δ 8.45 (d, J = 8.8 Hz, 1H), 7.84 (s, 1H), 6.96 (s, 1H), 6.35 (d, J = 8.8 Hz, 1H), 4.21 (s, 4H), 3.97 (s, 2H), 3.71 (s, 2H), 3.37-3.27 (m, 4H), 2.86 (t, J = 6.4 Hz, 2H), 2.77 (t, J = 6.0 Hz, 2H), 2.06-1.94 (m, 4H). ^{13}C NMR (101 MHz, CD_2Cl_2) δ 165.78, 159.46, 152.56, 147.51, 146.11, 145.21, 145.13, 144.95, 135.23, 126.07, 124.01, 119.58, 113.99, 107.70, 106.12, 102.91, 50.24, 49.82, 29.76, 27.50, 21.28, 20.36, 20.17. HRMS (ESI): m/z 299.1006 $[M+H]^+$ (calcd for $C_{14}H_{14}F_3N_2O_2^+$, 299.1002).

2.3. General procedure for spectroscopic studies

Studies were carried out in degassed phosphate-buffer (PB, 20 mM, pH 7.4).

Probes were dissolved into DMSO to prepare the stock solutions (5 mM). For the selectivity study, biologically relevant molecules were prepared as stock solutions of 500 mM, then appropriate amount of species were added to separate portions of the probe solution and mixed thoroughly. Each reaction mixture was shaken uniformly before emission spectra were measured. All measurements were performed in a 3 mL corvette with 2 mL solution. Excitation, 448 nm; emission, 496 nm. The fluorescent quantum yields for probes **1**, **1a**, **2** and **2a** were determined using 6-amino-2-butyl-1H-benzo[de]isoquinoline-1,3(2H)-dione (Φ = 0.13, PB, 20 mM, pH 7.4) as the standard substance [20]. Time-resolved fluorescence decay measurements were carried out at room temperature on a picosecond-diode-laser-based, time-correlated single-photon-counting (TCSPC) fluorescence spectrometer (FLS 980). All tested samples were dissolved in MeOH solution. All the decays were fitted to a double exponential function.

2.4. DFT calculations

DFT calculations of selected compounds were performed using the Gaussian 09 software package [21]. Geometry optimizations and unscaled frequency calculations were carried out at the B3LYP/6-31G* level of theory.

Compd.	HOMO/ev	LUMO/ev	ΔE/ev	λ_{ex}/nm	λ_{em}/nm	LOD/μM	Φ	τ(ns)
1	-5.78	-2.69	3.08	405	480	9	0.000073	ND
1a	-5.44	-1.61	3.83	405	480	/	0.017	3.53
2	-5.59	-2.69	2.90	449	496	0.9	0.00083	ND
2a	-5.19	-1.50	3.69	449	496	/	0.81	6.27

Table 1. Summary of frontier molecular orbital energy and optical properties of **1**, **1a**, **2**, **2a**.

2.5. Cell culture and fluorescence imaging

A549 cells were cultured at 37 ºC, 5% CO_2 in F12 supplemented with 10% fetal bovine serum (FBS), 100 U/ml penicillin, 100 μg/ml streptomycin, and 4 mM L-glutamine. HEK-293A cells were cultured at 37 ºC, 5% CO_2 in DMEM/HIGH GLUCOSE (GIBICO) supplemented with 10% fetal bovine serum (FBS), 100 U/ml penicillin, 100 μg/ml streptomycin, and 4 mM L-glutamine. The cells were

maintained in exponential growth, and then seeded in glass-bottom 35 mm plate at the density about 2 × 10^4 /well. Cells were passaged every 2-3 days and used between passages 3 and 10. For living cell imaging, cells were first incubated with Na_2S (100 μM) for 30 min at 37 °C. Then, removed the culture medium and washed the cells with PB (10 mM, pH 7.4) for three times, and treated with probe **2** (10 μM) for 30 min at 37 ºC. While the control cells were only treated with probe **2** at 37 ºC for 30 min. Emission was collected at green channel (510-550 nm) under 405 nm excitation.

2.6. Fluorescence imaging of zebrafish

Zebrafishes, 3-7 days postfertilization, were purchased from Eze-Rinka Company (Nanjing, China). The zebrafishes were cultured in 5 mL of embryo medium supplemented with 1-phenyl-2-thiourea (PTU) in 6-well plates for 24 h at 30 °C. Then the zebrafish was incubated with Na_2S (200 μM) or L-Cys (200 μM) for 4 h. After removed the embryo medium and washed the zebrafish with PB (10 mM, pH 7.4) for three times, the zebrafish was further incubated with probe **2** (10 μM) for 1 h at 30 °C, and then imaged.

3. Results and discussion

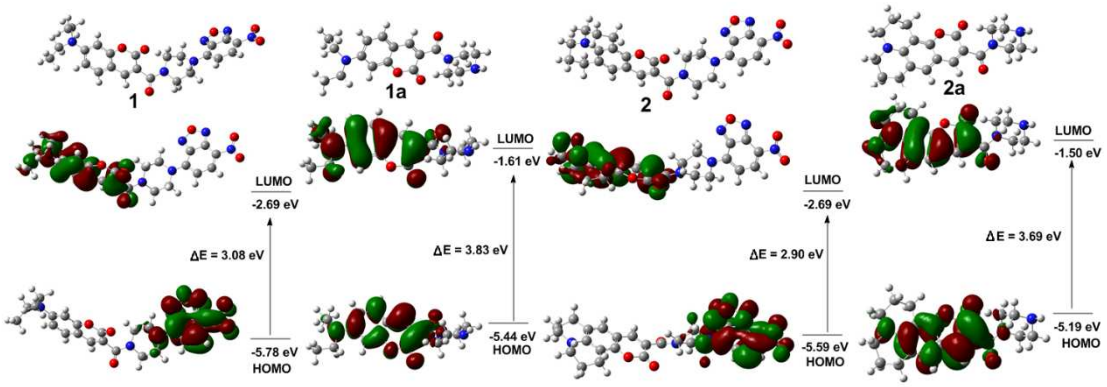

Fig. 1.Optimized structures and frontier orbital energy of **1**(a), **1a** (b), **2**(c), and **2a**(d). Data were calculated by Gaussian 09 with B3LYP/6-31G(d) level.

To better understand the superiority of probe **2** over probe **1** in this work, density functional theory (DFT) calculations were performed. As shown in Table 1 and Fig. 1, the energy difference (ΔE) of the highest occupied molecular orbital (HOMO) and the

lowest unoccupied molecular orbital (LUMO) of probes **1** and **2** are 3.08 eV and 2.90 eV, respectively, which are lower than that of **1a** (ΔE = 3.83 ev) and **2a** (ΔE = 3.69 ev), suggesting that fluorescence resonance energy transfer (FRET) could occur between coumarin and NBD within both probes. Fluorescence of coumarin and absorbance of NBD have an obvious overlap (Fig. S1), which also supports the possible occurrence of the FRET effect between the two fluorophores. The energy difference of fluorophore **2a** is lower than **1a**, suggesting that under light excitation, the electrons of **2a** in HOMO orbital can be more easily transferred to LUMO orbital than **1a** to give longer emission wavelength. Moreover, the electron-density in the HOMO or LUMO orbital is much different for **2a**, implying that there is an electron flow within coumarin with a large intramolecular charge transfer (ICT) effect. Inspired by the calculation results, we determined to synthesize probe **2** for H_2S sensing.

Probe **2** can be smoothly prepared in a five-step synthesis by using julolidine-fused phenyl 3-carbaldehydeas the starting material with a total yield of 47% (Scheme 2). The probe **2** was well characterized by ^{1}H and $^{13}C\{1H\}$ NMR spectroscopy as well as high-resolution mass spectrometry (HRMS). The sensing mechanism of the probe **2** should be the thiolysis of NBD amine [16], which was confirmed by HRMS (Fig. S2). The time-dependent absorbance spectra of **2** with H_2S also implied the thiolysis product NBS-SH (Fig. S3) [17b].

With probe **2** in hand, we first tested the fluorescence of probe **2** in the absence and presence of H_2S. The result showed that probe **2** exhibited nearly non-fluorescence (Φ = 0.00083) in the PB buffer (20 mM, pH 7.4) compared to that of its fluorophore **2a** (Φ = 0.81). This should be majorly due to the strong intramolecular FRET effect in **2**, though the photo-induced electron transfer (PET) between nitro group in NBD and coumarin could also contribute to a certain quenching effect [16d]. Upon reaction with H_2S, the FRET effect disappeared and significant fluorescence increase was observed for the probe **2**, implying the great potency for H_2S sensing. The emission peak of fluorophore **2a** was 496 nm, showing a notable red shift than that of **1a**.

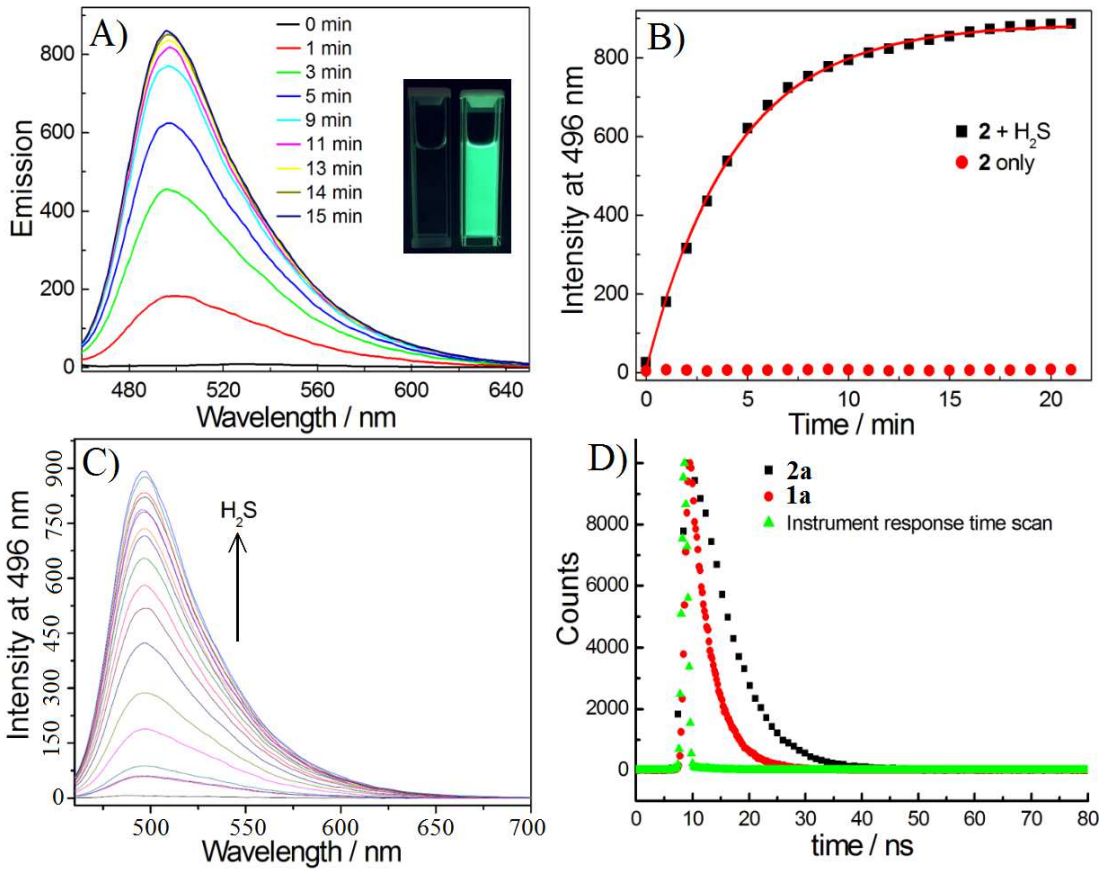

Fig. 2. (A) Time-dependent spectra change of **2** (5μM) when treated with Na_2S (500 μM) in PB buffer (20 mM, pH 7.4) at room temperature. Inset: photographs of **2** without (left) and with (right) Na_2S under UV analyzer (λ_{ex} = 365 nm). (B) Time-dependent fluorescent intensity at 496 nmof **2** in the absence (red dot) or presence (back dot) of H_2S.The red line represents the best fitting to give k_{obs} of 0.23 min^{-1}. (C) Spectra change of **2** (5 μM) when treated with Na_2S (0-500 μM) in PB buffer (20 mM, pH 7.4) at room temperature. (D) The fluorescence life-time of **1a** and **2a**.

Encouraged by the primary results, we examined the time-dependent fluorescence response of **2**with H_2S (Na_2S was used as an equivalent). As shown in Fig. 2A, a strong emission peak appeared at 496 nm. The fluorescent intensity of **2** increased about 40-fold within 1 min; and the fluorescence reached the steady state at 15 min with more than 200-fold intensity enhancement at 496 nm (Fig. 2B). The LOD of **2** for H_2S detection was determined as 0.9 μM using the $3\sigma/k$ method [16]. Compared to its parent probe **1**, probe **2** showed much improved response time (**1**: 45 min vs. **2**: 15 min), LOD (**1**: 9 μM vs. **2**: 0.9 μM) and fluorescent enhancement (**1**: 45 folds vs. **2**: 200 folds). Specifically, compared with **1a** (Φ = 0.017), the quantum yield of **2a** (Φ = 0.81) improved more than 47 folds, and the fluorescence life-time of **2a** (τ = 6.27 ns)

was also much longer than **1a** (τ = 3.53 ns) (Fig. 2D and Table 1). These data are consistent with the theoretical calculations, indicating that the twisting-blockage of N,N-diethylamino group can significantly improve the performances of the fluorescence probe **2**.

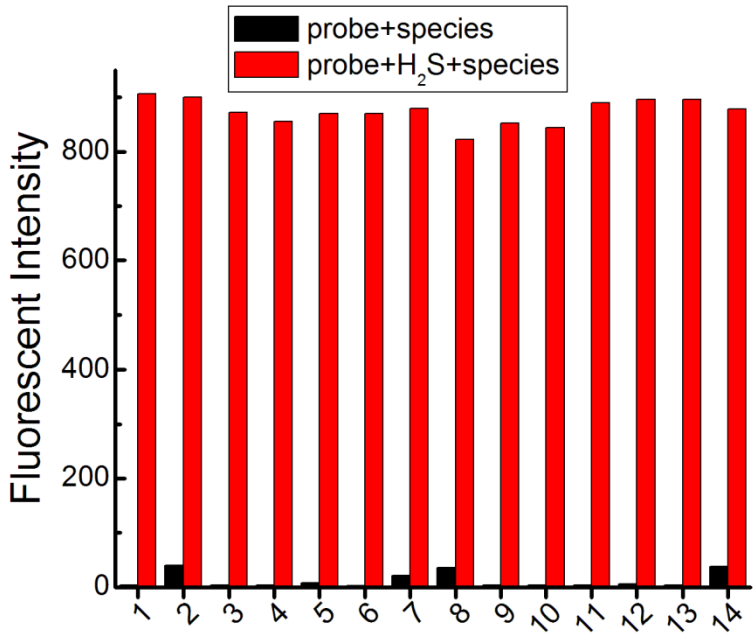

Fig. 3. Fluorescence intensity at 496 nm of **2** (5μM) upon reacting with species (1 mM, black bar) or H_2S and species (1 mM, red bar) in PB (pH 7.4) for 15 min: 1) **2** only; 2) SO_3^{2-}; 3) CH_3COO^-; 4) $C_2O_4^{2-}$; 5) F^-; 6) NO_2^-; 7) I^-; 8) HCO_3^-; 9) H_2O_2; 10) ClO^-; 11) Cys; 12) Hcy; 13) GSH; 14) mercaptoethanol.

One of the major requirements for a fluorescent probe is that it must exhibit a selective response towards the targeted analytes but not for other competing species. In order to confirm that the turn-on response of **2** was selectively caused by H_2S, we investigated the selectivity of **2** against other commonly encountered analytes (Fig. 3). Different biologically relevant species, such as SO_3^{2-}, mercaptoethanol, GSH, cysteine, Hcy, H_2O_2, ClO^-, CH_3COO^-, $C_2O_4^{2-}$, NO_2^-, F^-, I^- and HCO_3^- were evaluated. The results showed that probe **2** exhibited high selectivity toward H_2S among the selected analytes. Although four species (mercaptoethanol, HCO_3^-, I^- and SO_3^{2-}) induced a slight fluorescence enhancement, which was much lower in comparison with that of H_2S. We also tested the fluorescence of the probe with these analytes in the presence of H_2S (Fig. 3, red bar). The results implied that all analytes did not interfere with the

selective sensing of the probe toward H_2S. Furthermore, pH-dependent experiment indicated that **2** could sense H_2S within a wide pH range 6-11 (Fig. S4). Obviously, the largest fluorescence enhancement was appeared at around pH 7.4, suggesting that **2** could work efficiently at physiological conditions.

Inspired by the excellent properties of probe **2**, we further explored its feasibility in detection of H_2S in living biological systems. Firstly, methyl thiazolyl tetrazolium (MTT) assays were carried out, which indicated that **2** did not possess obvious cytotoxicity against HEK293A cells even at the concentration up to 20 μM (Fig. S5). Subsequently, we examined whether **2** could be used to detect intracellular H_2S in living cells. HEK293A cells were incubated with Na_2S (100 μM) for 30 min, washed by PB, then stained with **2** (10 μM) and imaged using a confocal fluorescence microscopy immediately. Cells incubated with **2** (10 μM) alone were used as control experiment. The results indicated that no fluorescence was observed for **2**-loaded cells (Fig. 4A), while cells treated with H_2S showed significantly bright green fluorescence (Fig 4B). Similar tests were also performed in A549 cells (Fig. 4C, 4D). The results suggest that probe **2** is cell-permeable and can be used for imaging of H_2S in both A549 and HEK293A cells.

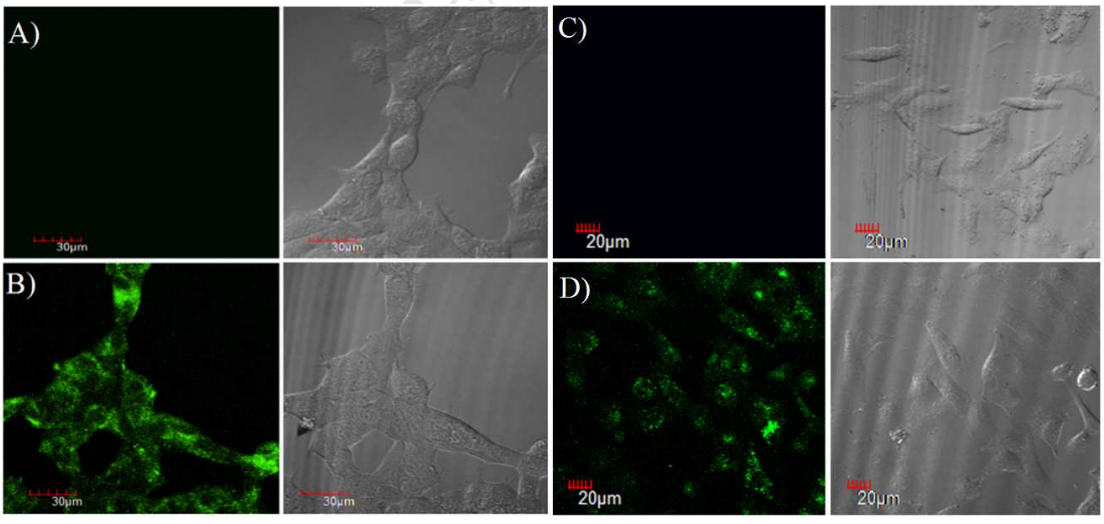

Fig. 4. Fluorescence images for exogenous H_2S detection in HEK293A and A549 cells using **2**. A) HEK293A Cells were incubated with **2** (10 μM) for 30 min and imaged in fluorescence (left) and bright field (right). B) HEK293A Cells were incubated with Na_2S (100 μM) for 30 min, washed, then treated with **2** (10 μM) for 30 min and imaged in fluorescence (left) and bright-field (right). C) A549 Cells were incubated with **2** (10 μM) for 30 min and imaged in fluorescence (left) and bright field (right). D) A549 Cells were incubated with Na_2S (100 μM) for 30 min, washed, then treated

with **2** (10 μM) for 30 min and imaged in fluorescence (left) and bright-field (right).

Encouraging with these results, we further determined the applicability of probe **2** in visualizing H_2S *in vivo*, and zebrafish larvae were selected as the biological model [19c]. The zebrafish was first incubated with **2** for 1 h, washed, and then treated with Na_2S (200 μM) for another 4 h. The zebrafish stained with **2** alone was used as control group. As shown in Fig. 5A, no obvious fluorescence was observed in the **2**-loaded control group, whereas a strong green fluorescence was seen in venter and eyes of the H_2S-treated zebrafish (Fig. 5B). These results imply that probe **2** can be used to visualize H_2S *in vivo*. To further explore the potential of **2** in sensing endogenous H_2S *in situ*, L-Cys (200μM) was introduced to the **2**-stained zebrafish. To our delight, a significant green fluorescence enhancement was observed in the eyes and the venter of the larva (Fig. 5C). The locations of H_2S in zebrafish observed by us are in consisted with the reported literature [24]. Taken together, the above results indicated that probe **2** is an effective tool for H_2S detection in the living organisms.

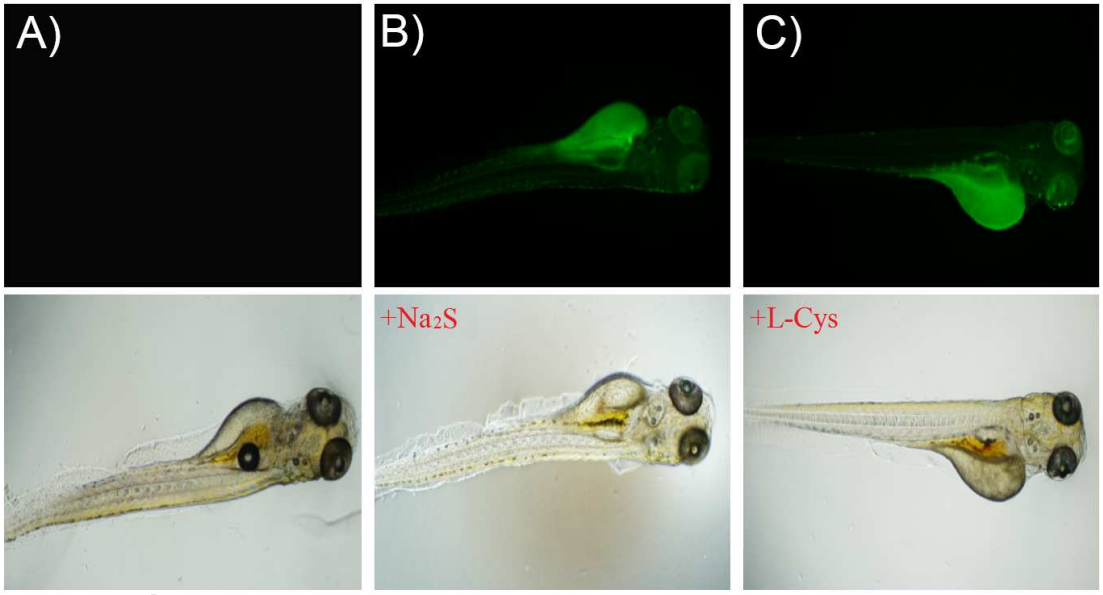

Fig. 5. Confocal microscopy images for exogenous and L-Cys-induced endogenous H_2S detection in zebrafish larvae. A) The zebrafish was incubated with probe **2** (10 μM) for 1 h and imaged in green field (up) and bright field (down). B) The zebrafish was incubated with probe **2** (10 μM) for 1 h, then with Na_2S (200 μM) for 4 h and imaged in green field (up) and bright field (down). C) The zebrafish was incubated with probe **2** (10 μM) for 1 h, then with L-Cys (200 μM) for another 4 h, and imaged in green field (up) and bright field (down).

4. Conclusion

In summary, we rationally designed a julolidine-fused coumarin-based probe **2** based on DFT calculations. This new probe is highly selective and sensitive towards H_2S, and can be used for H_2S detection in living cells and in zebrafish. Compared to its parent probe **1**, probe **2** shows significantly improved properties, including lower LOD, higher fluorescence response and higher sensitivity. This work further indicates that the twisting-blockage of N,N-diethylamino group can significantly improve the sensing performances of the fluorescence probes. Our work not only offers a useful strategy to enhance the properties of H_2S fluorescence probes, but also provides an excellent probe tool for imaging of H_2S in living biological systems.

Acknowledgements

This work was supported by the National Key R&D Program of China (2017YFD0200500, 16JCYBJC20200), NSFC (21702111), 111 project (B14004).

Appendix A. Supplementary data

Supplementary data related to this article can be found at http://dx.doi.org/10.1016/j.dyepig.2018.xx.xxx.

References

[1] a) Wang R. Physiological implictions of hydrogen sulfide: a whiff exploration that blossomed. Physiol Rev 2012;92:791-896;

b) Kabil O, Banerjee R. Enzymology of H_2S biogenesis, decay and signaling. Antioxid Redox Signal 2014;20:770-82;

c) Kolluru G K, Shen X, Bir S C, Kevil CG. Hydrogen sulfide chemical biology: pathophysiological roles and detection. Nitric Oxide 2013;35:5-20.

[2] a) Li L, Rose P, Moore PK. Hydrogen sulfide and cell signaling. Annu Rev Pharmacol Toxicol 2011;51:169-87;

b) Kimura H. Hydrogen sulfide: production, release, and functions. Amino Acids 2011;41:113-21;

c) Wei L, Yi L, Song F, Wei C, Wang B, Xi Z. FRET ratiometric probes reveal the chiral-sensitive cysteine-dependent H_2S production and regulation in living cells. Sci Rep 2014;4:639-45.

[3] a) Liu YH, Lu M, Hu LF, Wong PT, Webb GD, Bian JS. Hydrogen sulfide in the mammalian cardiovascular system. Antioxid Redox Signal 2012;17:141-85.

b) Yi L, Wei L, Wang R, Zhang C, Zhang J, Tan T, Xi Z. A dual-response fluorescent probe reveals the H_2O_2-induced H_2S biogenesis through a cystathionine β-synthase pathway. Chem

Eur J 2015;21:15167-72.

[4] a) Papapetropoulos A, Pyriochou A, Altaany Z, Yang G, Marazioti A, Zhou Z, Jeschke MG, Branski LK, Herndon DN, Wang R, Szabó C, Snyder S. Hydrogen sulfide is an endogenous stimulator of angiogenesis. Proc Natl Acad Sci USA 2009;106:21972-77.

b) Coletta C, Módis K, Szczesny B, Brunyánszki A, Oláh G., Rios EC, Yanagi K, Ahmad A, Papapetropouloos A, Szabo C. Regulation of vascular tone, angiogenesis and cellular bioenergetics by the 3-mercaptopyruvate sulfurtransferase/H_2S pathway: functional impairment by hyperglycemia and restoration by DL-α-lipoic acid. Mol Med 2015;21:1-14.

[5] Módis K, Ju Y, Ahmad A, Untereiner A, Altaany Z, Wu L, Szabó C, Wang R. S-sulfhydration of ATP synthase by hydrogen sulfide stimulates mitochondrial bioenergetics. Pharmacol Res 2016;113:116-24.

[6] Du J, Huang Y, Yan H, Zhang Q, Zhao M, Zhu M, Liu J, Chen SX, Bu D, Tang C, Jin H, Hydrogen sulfide suppresses oxidized low-density lipoprotein (ox-LDL)-stimulated monocyte chemoattractant protein 1 generation from macrophages via the nuclear factor κB (NF-κB) pathway. J Biol Chem 2014;289:9741-53.

[7] a) Szabo C. Gasotransmitters in cancer: from pathophysiology to experimental therapy. Nat Rev Drug Disc 2016;15:185-203;

b) Wu D, Si W, Wang M, Lv S, Ji A. Hydrogen sulfide in cancer: friend or foe? Nitric Oxide 2015;50:38-45;

c) Hellmich MR, Coletta C, Chao C, Szabo C. The therapeutic potential of cystathionine β-synthetase/hydrogen sulfide inhibition in cancer. Antioxid Redox Signal 2015;22:424-48.

[8] a) Hancock JT, Whiteman M. Hydrogen sulfide and cell signaling: team player or referee? Plant Physiol Biochem 2014;78:37-42;

b) Calderwood , Kopriva S. Hydrogen sulfide in plants: from dissipation of excess sulfur tomolecule. Nitric Oxide 2014;41:72-78;

c) Li ZG, Min X, Zhou ZH. Hydrogen sulfide: a signal molecule in plant cross-adaptation. Front Plant Sci 2016;7:1621;

d) Guo H, Xiao T, Zhou H, Xie Y, Shen W. Hydrogen sulfide: a versatile regulator of environmental stress in plants. Acta Physiol Plant 2016;38:1-13.

[9] a) Álvarez C, García I, Moreno I, Pérez ME, Crespo JL, Romero LC, Gotor C. Cysteine-generated sulfide in the cytosol negatively regulates autophagy and modulates the transcriptional profile in Arabidopsis. Plant Cell 2012;24:4621-34;

b) Laureano-Marin AM, Moreno I, Romero LC, Gotor C. Negative regulation of autophagy by sulfide is independent of reactive oxygen species. Plant Physiol 2016;171:1378-91.

[10] Jia H, Wang X, Dou Y, Liu D, Si W, Fang H, Zhao C, Chen S, Xi J, Li J. Hydrogen sulfide-cysteine cycle system enhances cadmium tolerance through alleviating cadmium-induced oxidative stress and ion toxicity in arabidopsis roots. Sci Rep 2016;6:39702.

[11] a) Lin VS, Chen W, Xian M, Chang C. Chemical probes for molecular imaging and detection of hydrogen sulfide and reactive sulfur species in biological systems. J Chem Soc Rev 2015;44:4596-4618;

b) Yu FB, Han XY, Chen LX. Fluorescent probes for hydrogen sulfide detection and bioimaging. Chem Commun 2014;50:12234-49;

c) Li J., Yin C, Huo F. Cheminform abstract: chromogenic and fluorogenic chemosensors for

hydrogen sulfide: review of detection mechanisms since the year 2009. RSC Adv 2015;5: 2191-206;

d) Xuan W, Sheng C, Cao Y, He W, Wang W. Fluorescent probes for the detection of hydrogen sulfide in biological systems. Angew Chem Int Ed 2012;51:2282-84;

e) Ding Y, Zhu WH, Xie Y. Development of ion chemosensors based on porphyrin analogues. Chem Rev 2017;117:2203-56;

f) Hartle MD, Pluth MD. A practical guide to working with H_2S at the interface of chemistry and biology. Chem Soc Rev 2016;45:6108-17.

[12] a) Qian Y, Karpus J, Kabil O, Zhang SY, Zhu HL, Banerjee R, Zhao J, He C. Selective fluorescent probes for live-cell monitoring of sulphide. Nat Commun 2011;2:495;

b) Qian Y, Zhang L, Ding ST, Deng X, He C, Zheng XE, Zhu HL, Zhao J. A fluorescent probe for rapid detection of hydrogen sulfide in blood plasma and brain tissues in mice. Chem Sci 2012;3:2920-23;

c) Chen YC, Zhu CC, Yang ZH, Chen JJ, He YF, Jiao Y, He WJ, Qiu L, Cen JJ, Guo ZJ, Chen Y. A ratiometric fluorescent probe for rapid detection of hydrogen sulfide in mitochondria. Angew Chem Int Ed 2013;52:1688-91;

d) Bu L, Chen J, Wei X, Li X, Agren H, Xie Y. An AIE and ICT based NIR fluorescent probe for cysteine and homocysteine. Dyes Pigments 2017;136:724-31;

e) Wang Q, Wei X, Li C, Xie Y. A novel *p*-aminophenylthiol- and cyano- substituted BODIPY as a fluorescence turn-on probe for distinguishing cysteine and homocysteine from glutathione. Dyes Pigments 2018;148:212-18;

f) Wang Q, Ma F, Tang W, Zhao S, Li C, Xie Y. A novel nitroethylene-based porphyrin as a NIR fluorescence turn-on probe for biothiols based on the Michael addition reaction. Dyes Pigments 2018;148:437-43.

[13] a) Lippert AR, New EJ, Chang CJ. Reaction-based fluorescent probes for selective imaging of hydrogen sulfide in living cells. J Am Chem Soc 2011;133:10078-80;

b) Wu MY, Li K, Hou JT, Huang Z, Yu XQ. A selective colorimetric and ratiometric fluorescent probe for hydrogen sulfide. Org Biomol Chem 2012;10:8342-47;

c) Xuan W, Pan R., Cao Y, Liu K, Wang W. A fluorescent probe capable of detecting H_2S at submicromolar concentrations in cells. Chem Commun 2012;48:10669-71;

d) Wei L, Zhu Z, Li Y, Yi L, Xi Z. A highly selective and fast-response fluorescent probe for visualization of enzymatic H_2S production in vitro and in living cells. Chem Commun 2015;51:10463-6;

e) Shi DT, Zhou D, Zang Y, Li, J, Chen GR, James TD, He XP, Tian H. Selective fluorogenic imaging of hepatocellular H_2S by a galactosyl azidonaphthalimide probe. Chem Commun 2015;51:3653-5;

[14] Sasakura K, Hanaoka K, Shibuya N, Mikami Y, Kimura Y, Komatsu T, Ueno T, Terai T, Kimura H, Nagano T. Development of a highly selective fluorescence probe for hydrogen sulfide. J Am Chem Soc 2011;133:18003-5.

[15] Cao XW, Lin WY, Zheng KB, He LW. A near-infrared fluorescent turn-on probe for fluorescence imaging of hydrogen sulfide in living cells based on thiolysis of dinitrophenyl ether. Chem Commun 2012;48:10529-10531.

[16] a) Wei C, Wei L, Xi Z, Yi L. A FRET-based fluorescent probe for imaging H_2S in living cells. Tetrahedron Lett 2013;54:6937-9;

b) Huang Y, Zhang C, Xi Z. Yi L. Synthesis and characterizations of a highly sensitive and selective fluorescent probe for hydrogen sulfide. Tetrahedron Lett 2016;57:1187-91;

c) Zhang K, Zhang J, Xi Z, Li LY, Gu X, Zhang QZ, Yi L. A new H_2S-specific near-infrared fluorescence-enhanced probe that can visualize the H_2S level in colorectal cancer cells in mice. Chem Sci 2017;8:2776-81;

d) Wang RY, Li ZF, Zhang CY, Li YY, Xu GC, Zhang QZ, Li LY, Yi L, Xi Z. Fast-response turn-on fluorescent probes based on thiolysis of NBD amine for H_2S bioimaging. ChemBioChem, 2016;17:962-68;

e) Zhang J, Wang RY, Zhu ZT, Yi L, Xi Z. A FRET-based ratiometric fluorescent probe for visualizing H_2S in lysosomes. Tetrahedron 2015;71:8572-6;

f) Song F, Li Z, Li J, Wu S, Qiu X, Xi Z, Yi L. Investigation of thiolysis of NBD amines for the development of H_2S probes and evaluating the stability of NBD dyes. Org Biomol Chem 2016;14:11117-24;

g) Pak YL, Li J, Ko KC, Kim G, Lee JY, Yoon J. Mitochondria-targeted reaction-based fluorescent probe for hydrogen sulfide. Anal Chem 2016;88:5476-81.

[17] a) Wei C, Zhu Q, Liu WW, Chen WB, Xi Z, Yi L. NBD-based colorimetric and fluorescent turn-on probes for hydrogen sulfide. Org BiomolChem 2014;12:479-85;

b) Montoya LA, Pearce TF, Hansen RJ, Zakharov LN, Pluth MD. Development of selective colorimetric probes for hydrogen sulfide based on nucleophilic aromatic substitution. J Org Chem 2013;78:6550-7;

c) Zhang C, Wu S, Xi Z, Yi L. Design and synthesis of NBD-S-dye dyads for fluorescently discriminative detection of biothiols and Cys/Hcy. Tetrahedron 2017; 73:6651-6;

d) Sun L, Jiang Y, Zhang C, Ji X, Lv D, Xi Z, Yi L. A NBD-S-rhodamine dyad for dual-colordiscriminative imaging of biothiols and Cys/Hcy. New J Chem 2018; 42:15277-83;

e) Lee D, Kim G, Yin J, Yoon J. An aryl-thioether substituted nitrobenzothiadiazole probe for the selective detection of cysteine and homocysteine. Chem Commun 2015;51:6518-20.

[18] Wang C, Cheng X, Tan J, Ding Z, Wang W, Yuan D, Li G, Zhang H, Zhang X. Reductive cleavage of C=C bonds as a new strategy for turn-on dual-fluorescence in effective sensing of H_2S. Chem Sci 2018;9:8369-74.

[19] a) Zhang H, Zhang C, Liu R, Yi L, Sun H. A highly selective and sensitive fluorescent thiol probe through dual-reactive and dual-quenching groups. Chem Commun 2015;51:2029-32;

b) Zhang C, Wei L, Zhang J, Wang RY, Xi Z, Yi L. A FRET-ICT dual-quenching fluorescent probe with large off-on response for H_2S: synthesis, spectra and bioimaging. ChemCommun 2015;51:7505-8;

c) Wei C, Wang RY, Zhang CY, Xu GC, Li YY, Zhang QZ, Li LY, Yi L, Xi Z. Dual Reactable Fluorescent Probes for Highly Selective and Sensitive Detection of Biological H_2S. Chem Asian J 2016;11:1376-81;

d) Zhang C, Wang R, Cheng L, Li B, Xi Z, Yi L. A redox-nucleophilic dual reactable probe for highly selective and sensitive detection of H_2S: synthesis, spectra and bioimaging. Sci Rep 2016;6:30148.

[20] Sun Q, Yang SH, Wu L, Dong QJ, Yang WC, Yang GF. Detection of intracellular selenol-containing molecules using a fluorescent probe with near-zero background signal. Anal Chem 2016; *88*:6084-6091.

[21] Caricato M, Trucks GW, Frisch MJ, Wiberg KB.Electronic Transition Energies: A study of the performance of a large range of single reference density functional and wave function methods on valence and rydberg states compared to experiment. J Chem Theory Comput 2010;6:370-83.

[22] Grimm JB, English BP, Chen J, Slaughter JP., Zhang Z, Revyakin A, Patel R, Macklin JJ, Normanno D, Singer RH, Lionnet T, Lavis LD. A general method to improve fluorophores for live-cell and single-molecule microscopy. Nat Methods 2015;12:244-50.

[23] a) Sun Q, Yang SH, Wu L, Yang WC, Yang GF. A Highly sensitive and selective fluorescent probe for thiophenol designed via a twist-blockage strategy. Anal Chem 2016;88:2266-72;
b) Li J, Zhang CF, Yang SH, Yang WC, Yang GF. A coumarin-based fluorescent probe for selective and sensitive detection of thiophenols and its application. Anal Chem 2014;86:3037-42.

[24] Hong J, Feng W, Feng G. Highly selective near-infrared fluorescent probe with rapid response, remarkable large Stokes shift and bright fluorescence for H_2S detection in living cells and animals. Sensor Actuat B-Chem 2018;262:837-44.

A new julolidine-fused coumarin-NBD probe for H_2S detection is rationally designed based on the DFT caculations.

This new probe exhibits faster and larger *off-on* response as well as higher sensitivity compared with the previous coumarin-NBD probe.

This new probe possesses excellent selectivity and good biocompatibility, which can be employed to image H_2S in living cells and in zebrafish.